Mixed Matrix Membranes with Surface Functionalized Metal–Organic Framework Sieves for Efficient Propylene/Propane Separation

Youdong Cheng, Biplab Joarder, Shuvo Jit Datta, Norah Alsadun, Daria Poloneeva, Dong Fan, Rushana Khairova, Anastasiya Bavykina, Jiangtao Jia, Osama Shekhah, Aleksander Shkurenko, Guillaume Maurin, Jorge Gascon, and Mohamed Eddaoudi*

Membrane technology, regarded as an environmentally friendly and sustainable approach, offers great potential to address the large energy penalty associated with the energy-intensive propylene/propane separation. Quest for molecular sieving membranes for this important separation is of tremendous interest. Here, a fluorinated metal–organic framework (MOF) material, known as KAUST-7 (KAUST: King Abdullah University of Science and Technology) with well-defined narrow 1D channels that can effectively discriminate propylene from propane based on a size-sieving mechanism, is successfully incorporated into a polyimide matrix to fabricate molecular sieving mixed matrix membranes (MMMs). Markedly, the surface functionalization of KAUST-7 nanoparticles with carbene moieties affords the requisite interfacial compatibility, with minimal nonselective defects at polymer–filler interfaces, for the fabrication of a molecular sieving MMM. The optimal membrane with a high MOF loading (up to 45 wt.%) displays a propylene permeability of $\approx$95 barrer and a mixed propylene/propane selectivity of $\approx$20, far exceeding the state-of-the-art upper bound limits. Moreover, the resultant membrane exhibits robust structural stability under practical conditions, including high pressures (up to 8 bar) and temperatures (up to 100 °C). The observed outstanding performance attests to the importance of surface engineering for the preparation and plausible deployment of high-performance MMMs for industrial applications.

1. Introduction

Energy-efficient hydrocarbon separations are of prime importance in the petrochemical industry. One archetypal example is the separation of propylene (C_3H_6) from the mixture of C_3H_6 and propane (C_3H_8) produced during the hydrocarbon cracking process. High-purity C_3H_6 is essential to produce practical petrochemical commodities, including various polypropylene-based elastomers and plastomers.[1] Conventional cryogenic distillation-based C_3H_6/C_3H_8 separation is an energy-intensive technology, requiring large tray numbers (n > 100) and high reflux ratios (12–20) due to the close boiling points and similar molecular sizes of these two components.[2] Unsurprisingly, the development of novel separation technologies, offering greater energy efficiency, lower capital cost, and smaller carbon footprint, is an ongoing quest in academia and industry alike.

Prominently, membrane separation processes, renowned to offer up to 90% energy savings in contrast to traditional cryogenic distillation, are of great potential for

Y. Cheng, B. Joarder, S. J. Datta, N. Alsadun, J. Jia, O. Shekhah,
A. Shkurenko, M. Eddaoudi
Functional Materials Design
Discovery and Development (FMD3)
Advanced Membranes & Porous Materials Center (AMPMC)
Division of Physical Sciences and Engineering
King Abdullah University of Science and Technology
Thuwal 23955-6900, Saudi Arabia
E-mail: mohamed.eddaoudi@kaust.edu.sa

The ORCID identification number(s) for the author(s) of this article can be found under https://doi.org/10.1002/adma.202300296

N. Alsadun
Department of Chemistry
College of Science
King Faisal University (KFU)
Al-Ahsa 31982-400, Saudi Arabia

D. Poloneeva, R. Khairova, A. Bavykina, J. Gascon
Advanced Catalytic Materials (ACM)
KAUST Catalysis Center (KCC)
Division of Physical Sciences and Engineering
King Abdullah University of Science and Technology
Thuwal 23955-6900, Saudi Arabia

D. Fan, G. Maurin
Institut Charles Gerhardt Montpellier (ICGM)
Université de Montpellier
CNRS
ENSCM
Montpellier 34095, France

**ADVANCED
SCIENCE NEWS**

www.advancedsciencenews.com

**ADVANCED
MATERIALS**

www.advmat.de

the looked-for energy-efficient C_3H_6/C_3H_8 separation in industry.[3] Nevertheless, pure polymeric membranes often suffer from the trade-off effect between their membrane permeability and selectivity, known as upper bound limits,[4] largely impeding their industrial implementation. Moreover, condensable gases, including both C_3H_6 and C_3H_8, can easily swell polymer chains under relatively high pressures, leading to severe plasticization and/or dilation in most polymeric membranes with some exceptions in fluoropolymers.[5] To overcome these daunting challenges, hybrid mixed matrix membranes (MMMs), composed of a continuous polymer phase and a dispersed inorganic/organic filler phase, offer great promise for the fabrication of high-performance membranes. Plausibly, MMMs can simultaneously exhibit the virtues of both phases, including the good processability and decent mechanical robustness of the polymer phase and the intrinsically high permeability and selectivity of the filler phase. It is to be noted that different types of fillers such as metal–organic frameworks (MOFs),[6] porous organic cages (POCs),[7] and multi-silver complexes,[8] have been used in MMMs for C_3H_6/C_3H_8 separation. Among them, MOFs, composed of metal ions/clusters and multidentate organic linkers, have attracted the most attention owing to their adjustable pore structures and rich chemical functionality. Nevertheless, the number of MOFs explored in MMMs for C_3H_6/C_3H_8 separation is scarce due plausibly to limited MOFs with molecular sieving ability for this important application.[6a,9] Moreover, the exposed inorganic nodes in MOFs may undermine the polymer–filler interfacial compatibility in MMMs, leading to severe filler aggregation and formation of nonselective voids in the resultant membranes at high filler loadings (e.g., >35 wt.%).[10] Therefore, we envision that the successful deployment of a molecular sieving MOF for C_3H_6/C_3H_8 separation entails a customized interfacial interaction between MOF fillers and the polymer matrix, for the design and fabrication of MMMs with superior C_3H_6/C_3H_8 separation performances.

Here we report the preparation of high-performance MMMs containing surface-functionalized MOF sieve fillers for efficient C_3H_6/C_3H_8 separation. KAUST-7, also known as NbOFFIVE-1-Ni, when used as an adsorbent, demonstrated an excellent molecular sieving property for C_3H_6/C_3H_8 separation.[11] Encouraged by its distinct size-sieving performance, we explored KAUST-7 as a promising molecular sieve filler in MMMs for C_3H_6/C_3H_8 separation. Specifically, KAUST-7, constructed by coordination bonds between Ni^{2+} cations, $(NbOF_5)^{2-}$ polyatomic anions, and pyrazine molecules, possesses narrow 1D channels with a window diameter of ≈3.22 Å.[12] Nonetheless, the dynamic rotation of both pyrazine molecules and polyatomic anions could adapt the pore-aperture to allow the selective diffusion/transport of C_3H_6 over C_3H_8 based on the molecular sieving mechanism. Suitably, nano-sized KAUST-7 particles were prepared by a co-solvent synthesis approach and incorporated into the polymer matrix to fabricate MMMs. 6FDA-DAM (6FDA: 2,2-bis(3,4-carboxyphenyl)hexafluoropropane dianhydride; DAM: diaminomesitylene) was chosen as the matrix polymer due to its high thermal and chemical stabilities, good mechanical strength, excellent processability, and relatively moderate C_3H_6/C_3H_8 separation performance.[9a] To further improve the dispersibility and polymer-affinity of MOF fillers in the membrane, KAUST-7 nanoparticles were functionalized with a N-heterocyclic car-

bene, 1,3-bis(2,4,6-diisopropylphenyl)imidazole-2-ylidene (IDip), to produce surface-functionalized materials denoted as KAUST-7-IDip. We previously demonstrated that this carbene functionalization strategy was successful in mitigating the compatibility issue in zeolitic imidazolate frameworks (ZIFs)-based MMMs.[6b] Contrary to polymer-coating strategies reported in the literature where MOF pores were partially blocked by coating polymers,[13] this facile carbene functionalization strategy permitted to effectively retain the overall porosity of MOF fillers as carbene moieties can only attach to unsaturated metal sites on the outer surface of the MOF, while not entering MOF channels because of their bulkiness. As illustrated in **Figure 1**a, contrary to the easy filler aggregation in KAUST-7-based MMMs (denoted as 6FDA-DAM/KAUST-7), MMMs containing KAUST-7-IDip fillers (denoted as 6FDA-DAM/KAUST-7-IDip) show improved interfacial interactions and better filler dispersion states. Consequently, simultaneous increases in both the C_3H_6 permeability and the C_3H_6/C_3H_8 selectivity can be achieved for the 6FDA-DAM/KAUST-7-IDip MMMs even at a filler loading of up to 45 wt.%, making them promising for practical C_3H_6/C_3H_8 separation in the petrochemical industry.

2. Results and Discussion

To gain insight into the binding of the IDip molecule to the KAUST-7 surface, first-principles calculations at the density functional theory (DFT) level were carried out on a representative cluster model of the MOF surface (Figure S1, Supporting Information) with Ni-exposed sites to meet the experimental condition that uses an excess of Ni salt during the MOF preparation. Figure 1b reveals that the IDip molecule coordinates to the outer-surface Ni site via its C atom with the formation of a strong Ni−C chemical bond (bond length of 1.97 Å) associated with an accumulation of a high electronic charge density between the two atoms. The transferred electrons, particularly from the Ni-d state, are delocalized along the Ni−C bond, as shown in Figure S2 (Supporting Information). Analysis of the projected density of states (PDOS) onto the atomic orbitals of the exposed Ni sites and C atoms of the IDip molecule (Figure S3, Supporting Information) evidenced that the Ni_{3d} and C_{2p} orbitals contribute the most to the Fermi level. The associated high surface binding energy of 191.0 kJ mol^{-1} in KAUST-7-IDip strongly supports the formation of a strong chemical bond between the carbene molecule and the edge of the MOF nanoparticle and the subsequent stabilization of this functionalized MOF. It should be noted that compared to our previous work for the ZIF-67-based structure, the calculated adsorption energy of the IDip molecule is more negative than that for the ZIF-67 system ($-160.2-\approx-171.7$ kJ mol^{-1}),[6b] highlighting that IDip-functionalized KAUST-7 exhibits higher stability and is more stable than the ZIF-67 system. Subsequently, a bottom-up synthesis method was developed to prepare KAUST-7 nanoparticles using co-solvents at a relatively mild temperature (see the Experimental Section in Supporting Information for details). The optimized synthesis method substantially differs from bulk crystal synthesis.[11] As-synthesized KAUST-7 nanoparticles were homogenous in shape and exhibited an average particle size of 60–80 nm determined by scanning electron microscopy (SEM) (Figure S4, Supporting Information). Nano-sized MOF particles are preferred as filler materials
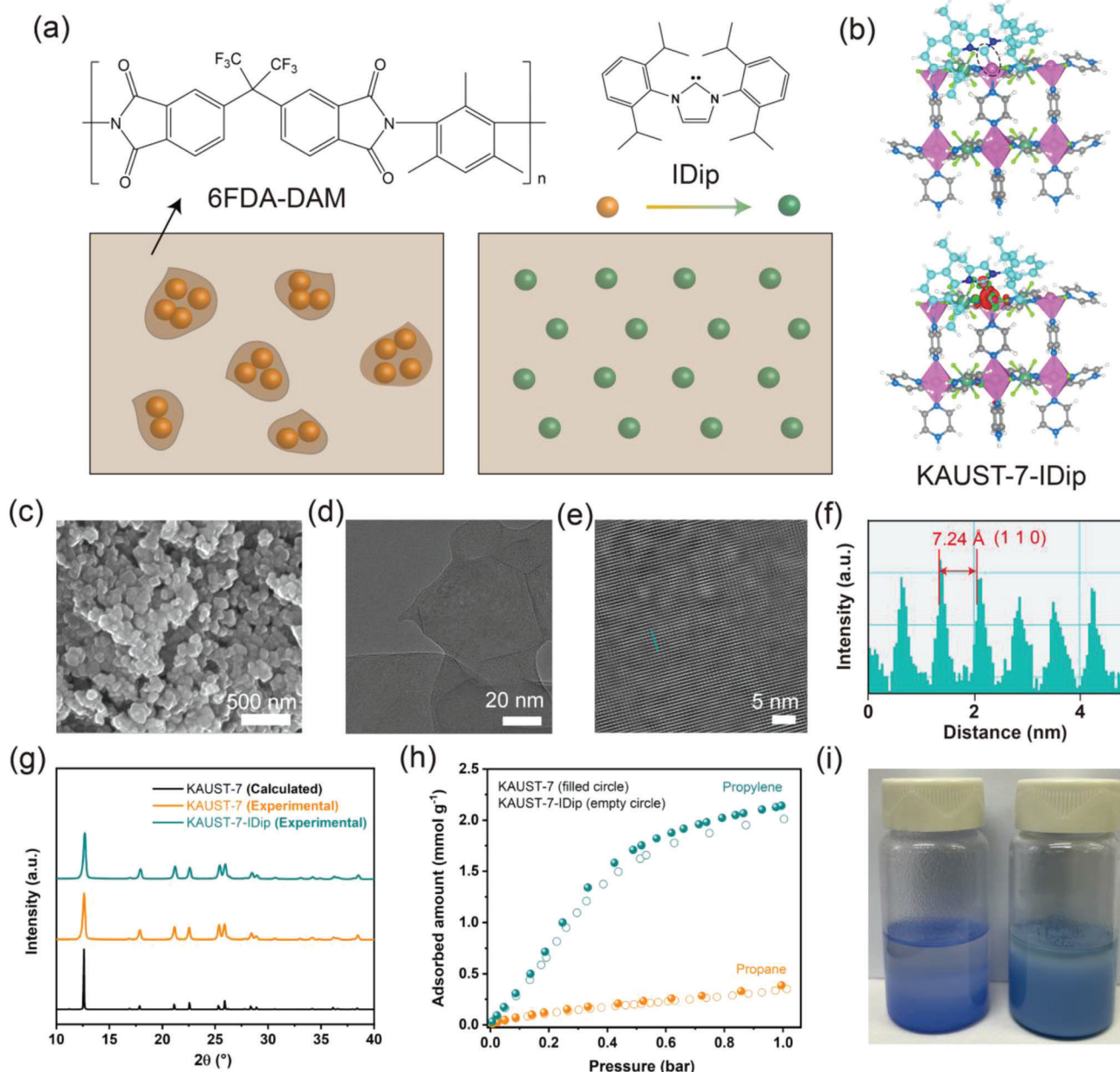
Figure 1. a) Schematic illustration of the preparation of MMMs using KAUST-7 and KAUST-7-IDip fillers. Fillers can easily agglomerate in KAUST-7-based MMM (left) and homogeneously dispersed in the matrix in KAUST-7-IDip-based MMM (right) owing to better polymer–filler interfacial compatibility in the latter. b) DFT-optimized KAUST-7-IDip structure model (top) and the corresponding electronic charge difference map (bottom). The formation of a chemical bond between the exposed Ni at the KAUST-7 surface and the IDip molecule is highlighted by a black dashed circle. The red color represents charge accumulation, and the green color represents charge depletion. Color code: IDip, C, cyan; H, white; N, blue; KAUST-7, C, grey; H, white; N, blue; Nb, green; F/O, lime; Ni octahedron, pink. c) SEM image of KAUST-7-IDip nanoparticles. d) HRTEM and e) enlarged HRTEM images of KAUST-7 nanoparticles. f) The corresponding distance profile analysis of (e), showing a periodic lattice structure. g) PXRD patterns of simulated KAUST-7, pristine KAUST-7 and KAUST-7-IDip. h) C_3H_6 and C_3H_8 adsorption isotherms for MOF fillers collected at 298 K and 1 bar. i) Optical images of KAUST-7 (left) and KAUST-7-IDip (right) in mesitylene after being first sonicated for 30 min and then allowed to settle for 24 h.

in MMMs compared to their micro-sized counterparts mainly due to their larger surface area-to-volume ratio that permits better polymer–filler interactions. KAUST-7-IDip nanoparticles were prepared by continuously stirring KAUST-7 nanoparticles in a mesitylene solution of the carbene ligand. It is to be noted that no alteration of particle size or morphology of the nanoparticles was

observed during the functionalization process (Figure 1c). The good crystallinity of as-synthesized KAUST-7 nanoparticles was confirmed by high-resolution transmission electron microscopy (HRTEM) (Figure 1d). Ordered lattice fringes can be clearly observed in an enlarged HRTEM image (Figure 1e), showing a periodic distance of 7.24 Å ascribed to the (1 1 0) plane of KAUST-7

crystals (Figure 1f). The crystallinity of the pristine KAUST-7 and KAUST-7-IDip nanoparticles was further evaluated using powder X-ray diffraction (PXRD) (Figure 1g). Both materials showed strong and identical diffraction peaks that match well with the simulated pattern of the KAUST-7 crystal structure, corroborating their good crystallinity and high phase purity.

X-ray photoelectron spectroscopy (XPS) offered supportive information on the surface functionalization of the MOF. The increase in C/Ni, C/Nb, and C/F atomic ratios provides evidence of the outer surface functionalization of carbene moieties in KAUST-7-IDip (Figure S5 and Table S1, Supporting Information). Moreover, attenuated total reflection Fourier transform infrared spectroscopy (ATR-FTIR) showed bands between 1630–1660 cm^{-1}, corresponding to the C=C stretching of pyrazine linkers in KAUST-7, with largely reduced intensity for KAUST-7-IDip owing to the capping of carbene moieties (Figure S6, Supporting Information). KAUST-7-IDip nanoparticles also exhibited weak bands between 2860–2960 cm^{-1} ascribed to the C–H stretching of IDip, which were absent in the pristine KAUST-7. It is of note that KAUST-7 is nonporous to N_2 at 77 K owing to its contracted pore size at this low cryogenic temperature. Fortunately, KAUST-7 adsorbs CO_2 at 273 K; consequently, this probe was employed to explore the porosity properties of KAUST-7 and KAUST-7-IDip. Based on the CO_2 adsorption isotherm at 273 K (Figure S7, Supporting Information), the apparent surface area and the pore volume of KAUST-7-IDip were estimated to be 208 $m^2 g^{-1}$ and 0.079 $cm^3 g^{-1}$, respectively, which are slightly lower than those of KAUST-7 (224 $m^2 g^{-1}$ and 0.085 $cm^3 g^{-1}$, respectively). The minor reduction in both the apparent surface area and the pore volume could be mainly caused by the attachment of nonporous carbene molecules in KAUST-7-IDip. Moreover, the pore size distribution data derived from the CO_2 adsorption isotherm highlighted that both KAUST-7 and KAUST-7-IDip showed the same average pore size of ≈3.46 Å. These results strongly corroborate the successful anchoring of IDip molecules on the outer surface of MOF nanoparticles in KAUST-7-IDip.

Adsorption isotherms of C_3H_6 and C_3H_8 were collected at 298 K for both KAUST-7 and KAUST-7-IDip and compared in Figure 1h and Figure S8 (Supporting Information). KAUST-7 showed obviously higher uptakes for C_3H_6 over C_3H_8, validating its size-sieving ability derived from its well-defined narrow channels. Notably, KAUST-7-IDip exhibited similar adsorption isotherms compared to KAUST-7, confirming the maintenance of internal porosity after IDip modification. The C_3H_6 uptake capacity only experienced a minor reduction from 2.13 mmol g^{-1} in KAUST-7 to 2.01 mmol g^{-1} in KAUST-7-IDip, which proves that the outer surface IDip functionalization hardly affects the adsorption properties of MOF nanoparticles. Moreover, at low C_3H_6 coverage, the isosteric heat of adsorption (Q_{st}) value in KAUST-7-IDip (43 kJ mol^{-1}) was very close to that in KAUST-7 (42 kJ mol^{-1}) (Figure S9, Supporting Information), further validating that IDip molecules barely interact with C_3H_6 molecules. Contrary to their similar adsorption properties, KAUST-7 and KAUST-7-IDip showed stark dispersibility differences in mesitylene. As shown in Figure 1i, KAUST-7 is non-dispersible in mesitylene and settles at the bottom, while KAUST-7-IDip can form a stable suspension in mesitylene under identical conditions. Notably, the greatly improved solvent dispersibility of

KAUST-7-IDip nanoparticles is key to their homogeneous dispersion in the polymer matrix in MMMs.[14]

Both KAUST-7 and KAUST-7-IDip nanoparticles were separately incorporated into 6FDA-DAM to fabricate MMMs via a solution casting method. To maximize the efficacy of MOF fillers in the membrane, achieving high filler loadings without deteriorating the membrane mechanical integrity is highly desired. Nevertheless, for a large number of reported MOF-based MMMs, their maximum filler loadings are kept below 35 wt.%, beyond which severe filler aggregation may easily lead to brittle membranes with largely reduced selectivity.[15] Various loadings of MOF fillers have been explored in this study. The actual filler loading matches well with the theoretical loading as confirmed by thermogravimetric analysis (TGA) of the membranes (Figure S10 and Tables S2 and S3, Supporting Information). The maximum filler loading for MMMs with KAUST-7-IDip could reach up to 45 wt.%, which is higher than the observed optimal value (≈30 wt.%) of MMMs with KAUST-7. The membrane with a even higher KAUST-7-IDip loading of 50 wt.% became too brittle and was difficult to handle for gas separation studies. The membrane microenvironment and polymer–filler interfacial micromorphology were characterized by SEM (**Figure 2**a; Figures S11 and S12, Supporting Information). Sharp differences between MMMs with different fillers can be easily observed, especially at high magnifications. KAUST-7-IDip nanoparticles are evenly distributed through the membrane even at a high loading of 45 wt.% without noticeable agglomeration or sedimentation. On the contrary, KAUST-7 nanoparticles exhibit filler aggregation when the loading amount reaches above 30 wt.%, suggesting their relatively less favored interactions with the matrix polymer. Moreover, optical images of MMMs corroborate the distinct dispersion characteristics of the two fillers (Insert in Figure 2a). The 6FDA-DAM/KAUST-7-IDip-45 wt.% MMM shows a flat surface and homogeneous color, while the MMM with a 40 wt.% loading of KAUST-7 exhibits a curved surface and uneven color. The energy-dispersive X-ray spectroscopy (EDS) mapping provides further evidence of the good distribution of KAUST-7-IDip in the membrane with a filler loading of up to 45 wt.% (Figure 2b). The signals of Ni, Nb, and F, elements solely from the KAUST-7-IDip, are detected evenly in the membrane, while the signal of C is distributed homogeneously throughout the whole membrane due to its presence in both MOF and polymer matrix, validating the excellent dispersion characteristics of the KAUST-7-IDip filler.

The crystallinity of MOF fillers in MMMs was probed by membrane XRD measurements (Figure 2c; Figure S13, Supporting Information). A broad diffraction peak between 10 and 20° is observed in a pure 6FDA-DAM membrane, highlighting its amorphous nature. As the loadings of both KAUST-7 and KAUST-7-IDip increase in the membrane, the intensities of characteristic diffraction peaks originating from MOF fillers gradually become prominent in all MMMs. This indicates that MOF fillers maintained their good crystallinity during the membrane preparation process. Moreover, dynamic mechanical analyses (DMA) were performed on all membranes to test their mechanical properties (Figure 2d; Figure S14, Supporting Information). The pristine 6FDA-DAM membrane shows a Young's modulus of 1.3 GPa, which is in good agreement with literature data (1.1–1.4 GPa).[7,16] For KAUST-7-based MMMs, their Young's modulus values gradually increase with increasing filler loadings
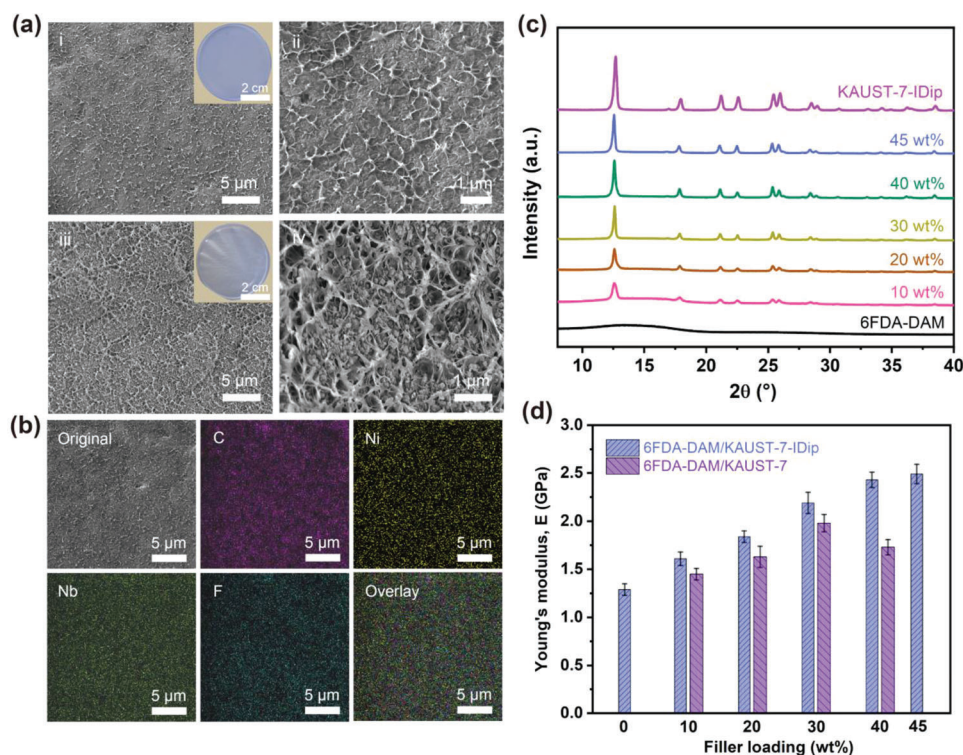
**ADVANCED
SCIENCE NEWS**

www.advancedsciencenews.com

**ADVANCED
MATERIALS**

www.advmat.de

Figure 2. a) Cross-sectional SEM images of 6FDA-DAM/KAUST-7-IDip-45 wt.% MMM (i,ii) and 6FDA-DAM/KAUST-7-40 wt.% MMM (iii,iv). Insert show the optical images of associated membranes. b) EDS mapping of 6FDA-DAM/KAUST-7-IDip-45 wt.% MMM. c) XRD patterns of KAUST-7-IDip nanoparticles and associated membranes with different filler loadings. d) Mechanical properties of KAUST-7-based and KAUST-7-IDip-based MMMs with different filler loadings.

before 30 wt.% and abruptly drop at a 40 wt.% loading, which can be ascribed to filler aggregation and formation of voids at this high loading as confirmed by SEM (vide supra). On the contrary, MMMs with KAUST-7-IDip exhibit continuously increased Young's modulus with the increment of filler loadings up to 45 wt.% owing to the anticipated good polymer–filler interfacial compatibility induced by carbene functionalization. The maximum Young's modulus in KAUST-7-IDip-based MMMs is 2.5 GPa, which is ≈90% and ≈25% higher than that of the pure polymeric membrane and the optimal KAUST-7-based MMM (30 wt.%). Furthermore, these increased modulus values indicate the enhanced rigidity of polymer chains in MMMs, which will plausibly promote the membrane anti-plasticization ability for separation applications at high pressures.[17]

The C_3H_6 and C_3H_8 adsorption isotherms of KAUST-7-IDip-based MMM with the maximum filler loading (45 wt.%) were collected at 298 K and compared with those of pure 6FDA-DAM membrane and KAUST-7-IDip nanoparticles (Figure S15, Supporting Information). With the incorporation of KAUST-7-IDip nanoparticles into the polymer matrix, the C_3H_8 uptake in the resultant MMM substantially decreases at 1 bar, while the effect on the C_3H_6 uptake is nominal. In addition, the pure KAUST-7-IDip nanoparticles show relatively reduced C_3H_6 and C_3H_8 sorption capacities in contrast to the pure polymeric membrane at the low-pressure range (0–0.2 bar) owing to their narrow channels. Therefore, the gas uptake capacities of the MMM fall between values of pure 6FDA-DAM membrane and KAUST-7-IDip

nanoparticles in the low-pressure regime. It is worth noting that a strong hysteresis exists in the C_3H_8 desorption isotherm for the MMM, highlighting the hindered diffusion of C_3H_8 molecules. This further confirms the enhanced sieving ability of the MMM, translating the unique properties of KAUST-7 associated with its modular narrow channels.

To evaluate the C_3H_6/C_3H_8 separation performance of resultant membranes, both single-gas and mixed-gas permeation measurements were conducted at 35 °C and detailed results are shown in **Figure 3**a,b and Tables S4 and S5 (Supporting Information). As anticipated and in accordance with previous reports,[6a,b,18] the incorporation of porous fillers with size-selective pores leads to a simultaneous increase in both permeability and selectivity. For KAUST-7-based MMMs, their C_3H_6/C_3H_8 selectivity reaches a maximum value at a filler loading of 30 wt.%. Adding more KAUST-7 nanoparticles results in enhancing the membrane permeability associated with a largely reduced selectivity, attributed as discussed above to the plausible presence of nonselective voids induced by fillers aggregation. For KAUST-7-IDip-based MMMs, the good interphase compatibility, promoted by carbene functionalization, results in a stepwise improvement in membrane separation properties for the entire loading range studied. The optimal MMM with a 45 wt.% of KAUST-7-IDip loading displays a C_3H_6 permeability of ≈95 barrer and a mixed C_3H_6/C_3H_8 selectivity of ≈20 at a feed pressure of 4 bar, overcoming the upper bound limits and surpassing most MOF-based membranes reported in the literature. Moreover, the
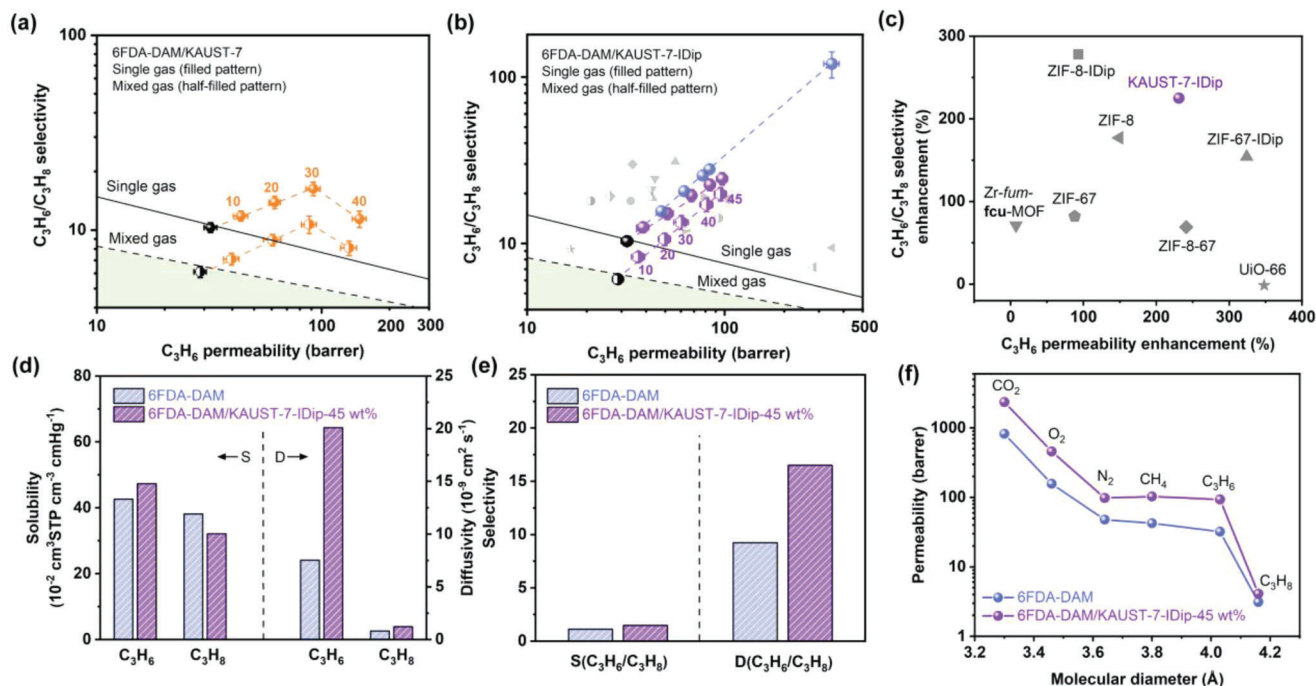
Figure 3. Single- and mixed-gas C_3H_6/C_3H_8 separation performance of a) 6FDA-DAM/KAUST-7 MMMs and b) 6FDA-DAM/KAUST-7-IDip MMMs with different filler loadings. Filled and half-filled patterns represent gas separation data obtained from single- and mixed-gas permeation measurements, respectively. Dashed lines are guides to highlight the membrane performance change by adding MOF fillers. Blue points in (b) show the theoretical performance data of MMMs with KAUST-7-IDip predicted by the Maxwell equation. c) A direct comparison of membrane performance change by adding MOF fillers for MMMs with KAUST-7-IDip and other MOFs in the literature. d) Solubility (left) and diffusivity (right), e) solubility selectivity (left) and diffusivity selectivity (right) of pure 6FDA-DAM membrane and 6FDA-DAM/KAUST-7-IDip-45 wt.% MMM. f) Single-gas permeability of pure 6FDA-DAM membrane and 6FDA-DAM/KAUST-7-IDip-45 wt.% MMM.

enhanced polymer–filler interaction affords minimized voids or defects in KAUST-7-IDip-based MMMs, permitting the back-calculation of intrinsic separation properties of MOF fillers based on the Maxwell equation.[19] This back-calculation approach was proven appropriate in providing reasonable estimations of intrinsic permeation properties of porous fillers when the filler loading in MMMs is low.[6a,10d,20] As shown in Figure 3b, a good match between experimental and calculated results is observed in KAUST-7-IDip-based MMMs when filler loadings do not exceed 30 wt.%. Nevertheless, at higher loadings, MMMs show a larger C_3H_6 permeability and a slightly lower C_3H_6/C_3H_8 selectivity that deviate from the calculated data, presumably attributed to the emergence of fast gas transport channels in the percolative network of MOF fillers at sufficiently high loadings (e.g., >40 wt.%).[21] Presumably, KAUST-7-IDip is anticipated to show a high C_3H_6 permeability of ≈350 barrer with an excellent C_3H_6/C_3H_8 selectivity of ≈120. Notably, this selectivity is close to the values of some well-known MOFs with size-sieving pores for C_3H_6/C_3H_8 separation, such as ZIF-8 (≈125) and Zr-*fum*-**fcu**-MOF (≈110).[6b,9b]

It is worth mentioning that all membranes experienced decreases in both gas permeability and selectivity when the membrane testing mode was switched from single-gas to mixed-gas measurement. This phenomenon can be attributed to the competitive sorption of C_3H_6 and C_3H_8 in the membrane as well as polymer swelling induced by these two condensable gases, as widely observed in other 6FDA-DAM-based membranes.[6b,9b,c] The mixed-gas C_3H_6/C_3H_8 selectivity of pure 6FDA-DAM membrane was reduced by 40.8%, whereas in the cases of MMMs with KAUST-7 (40 wt.%) or KAUST-7-IDip (45 wt.%) only 28.9% and 19.2% losses were observed, respectively. The addition of MOF fillers reduces chain mobility and increases rigidity of the matrix polymer, resulting in improved anti-swelling ability of the whole membrane. The better interfacial compatibility in KAUST-7-IDip-based MMMs further reinforces this effect, as validated by the minimum mixed-gas selectivity loss in all membranes. Moreover, to systematically evaluate the importance of KAUST-7-IDip on the membrane overall performance, permeability, and selectivity enhancement percentages were calculated based on separation data of pure 6FDA-DAM membrane and the corresponding MMMs with MOF fillers (Figure 3c). Markedly, KAUST-7-IDip outperforms many other well-known MOFs and is comparable to the state-of-the-art filler materials in the literature.[6a,b] The simultaneously improved permeability and selectivity in KAUST-7-IDip-based MMMs unambiguously suggest the existence of fast and molecular sieving channels in resultant membranes offered by MOF fillers.

To gain a better understanding of the detailed transport mechanism of KAUST-7-IDip-based MMMs, the membrane permeability (P_i) was deconvoluted into the product of diffusivity (D_i) and solubility (S_i) based on the solution-diffusion model (Figure 3d,e).[22] Contrary to the enhanced solubility of C_3H_6, the solubility of C_3H_8 is reduced in the MMM upon adding 45 wt.% of KAUST-7-IDip, resulting in marginally increased solubility selectivity. This strongly correlates to gas sorption results in both
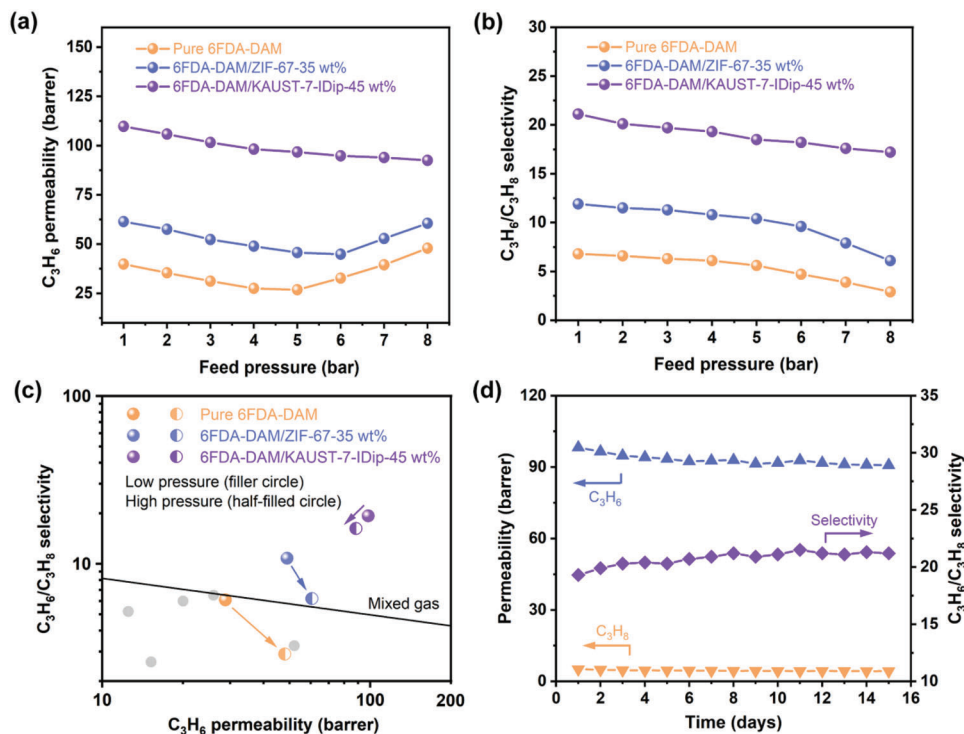
**ADVANCED
SCIENCE NEWS**

www.advancedsciencenews.com

**ADVANCED
MATERIALS**

www.advmat.de

Figure 4. a) C_3H_6 permeability b) C_3H_6/C_3H_8 selectivity of pure 6FDA-DAM membrane, 6FDA-DAM/ZIF-67-35 wt.% MMM, and 6FDA-DAM/KAUST-7-IDip-45 wt.% MMM as a function of the feed pressure (1–8 bar, C_3H_6/C_3H_8: 50/50, 35 °C). c) Mixed-gas C_3H_6/C_3H_8 separation performance change on the upper bound plot for different membranes as the feed pressure increases from a low pressure (4 bar) to a high pressure (8 bar). d) Long-term stability of 6FDA-DAM/KAUST-7-IDip-45 wt.% MMM at a feed pressure of 4 bar and 35 °C.

membranes and MOF nanocrystals. Remarkably, with the addition of KAUST-7-IDip, the membrane C_3H_6 diffusivity is greatly improved due to fast diffusion pathways created by intrinsic pores in the MOF structure, whereas the C_3H_8 diffusivity is only marginally increased presumably through percolative networks of MOF nanoparticles.[21,23] Consequently, a prominent increase in the membrane diffusivity selectivity is observed in the resultant MMMs. In summary, the simultaneously enhanced permeability and selectivity of MMMs are attributed to the fast and efficient molecular sieving pathways offered by KAUST-7-IDip nanocrystals in membranes. In addition, to clearly elucidate the gas sieving ability of MOF fillers, both pure 6FDA-DAM membrane and 6FDA-DAM/KAUST-7-IDip-45 wt.% MMM were examined for single-gas permeation of different gases with various molecular diameters, including CO_2, O_2, N_2, CH_4, C_3H_6, and C_3H_8 (Figure 3f). The permeability of nearly all gases, except C_3H_8, is enhanced noticeably in the membrane with the addition of KAUST-7-IDip, corroborating the impact of the high porosity of MOF fillers on the evaluated gases transport. Importantly, a clear cut-off between C_3H_6 and C_3H_8 is observed in the MMM, which unambiguously validates the molecular sieving property of KAUST-7-IDip.

To explore the potential implementation of KAUST-7-IDip-based MMMs for practical C_3H_6/C_3H_8 separation, where a high feed pressure is routine,[1] we evaluated the gas separation performance of resultant membranes at high pressures of up to 8 bar. For pure polymeric membranes, with the increase of the feed pressure to a certain level, condensable gases, including

C_3H_6 and C_3H_8, tend to dissolve more inside the membrane and swell polymer chains, causing a fast membrane permeability increase and a large selectivity loss. This phenomenon is known as "plasticization", and the corresponding pressure is termed "plasticization pressure". Both the optimal KAUST-7-IDip-based MMM and pure 6FDA-DAM membrane were tested at various pressures ranging from 1 to 8 bar. Moreover, as a comparison, a hybrid membrane containing the benchmark filler material for C_3H_6/C_3H_8 separation, ZIF-67,[6b] was also prepared, characterized, and examined under identical conditions (Figure S16, Supporting Information). As shown in **Figure 4**a,b, all membranes exhibit simultaneously reduced C_3H_6 permeability and C_3H_6/C_3H_8 selectivity with the increase of feed pressure in a low-pressure range (e.g., 1–5 bar), which can be attributed to the gradual saturation of Langmuir sites in the membrane at higher pressures based on the dual-mode sorption model.[17a] Pure 6FDA-DAM membrane shows a plasticization pressure of 5 bar, beyond which the membrane selectivity experiences a fast drop with the increase of the feed pressure. With the incorporation of 35 wt.% of ZIF-67 fillers, the membrane still plasticizes despite that the plasticization pressure is slightly improved to 6 bar. In addition, the "gate-opening" phenomenon in ZIF-67-based membranes under high pressure, due to rotation behavior of the organic linker in ZIF-67, contributes to the observed fast membrane selectivity loss.[24] On the contrary, the 6FDA-DAM/KAUST-7-IDip MMM shows relatively superior anti-plasticization performance even at a feed pressure of up to 8 bar. Plausibly, the interfacial compatibility in KAUST-7-IDip-based MMMs contributed to the

2300296 (7 of 9)

improved membrane anti-plasticization ability, resulting from the lessened polymer chain mobility and increased chain stiffness. Distinctly, KAUST-7-IDip features relatively rigid 1D channels instead of flexible pore windows in ZIF-67, therefore it can maintain the size-sieving ability under higher pressures, as corroborated by our previous finding showing a larger adsorption capacity of C_3H_6 over C_3H_8 in KAUST-7 even at a pressure of up to 7 bar.[11] This is in stark contrast to the almost identical uptake capacity of C_3H_6 and C_3H_8 in ZIF-67 at a low pressure of 1 bar.[9b] Consequently, suffering from the plasticization phenomenon, the pure 6FDA-DAM membrane and ZIF-67-based MMM exhibit 48% and 57% decreases in selectivity when the feed pressure is elevated from 1 to 8 bar, respectively, whereas the MMM with KAUST-7-IDip only shows an 18% selectivity loss under identical conditions. A clear trend in the performance change of different membranes as the feed pressure increases from 4 to 8 bar is shown in Figure 4c. Both pure 6FDA-DAM membrane and the ZIF-67-based MMM become less attractive for high-pressure C_3H_6/C_3H_8 separation, while our high-loading KAUST-7-IDip-based MMM still shows a promising separation performance that largely overcomes the upper bound limit as the feed pressure reaches 8 bar, highlighting its prospective implementation for industrial applications.

The mixed-gas separation performances of KAUST-7-IDip-based MMM and pure 6FDA-DAM membrane were further evaluated at varying temperatures ranging from 35 to 100 °C (Figure S17, Supporting Information). Both membranes show monotonically reduced C_3H_6/C_3H_8 selectivity as temperature increases due to the faster enhancement in diffusivity for larger gas molecules (C_3H_8) over smaller gas molecules (C_3H_6) at higher temperatures.[6c] Nevertheless, even at 100 °C, the MMM still shows a good selectivity of 16.4, much higher than that of pure 6FDA-DAM (3.8), validating its notable separation performance at high temperatures. In addition, the long-term stability of the KAUST-7-IDip-based MMM was assessed by exposing the membrane to a continuous C_3H_6/C_3H_8 gas flow for 15 days, while no evident performance degradation was observed (Figure 4d), further demonstrating the positive effect of MOF functionalization.

3. Conclusion

We have demonstrated the design and preparation of high-performance MMMs with size-selective MOF fillers for efficient C_3H_6/C_3H_8 separation. A carbene functionalization strategy was successfully employed to improve the interfacial compatibility and minimize nonselective defects in hybrid membranes. The carbene functionalization process only occurs on the outer surface of MOF nanoparticles, therefore maintaining the size-sieving channels of MOF fillers accessible to target gas molecules. KAUST-7-IDip-incorporated MMMs demonstrate simultaneously enhanced C_3H_6 permeability and C_3H_6/C_3H_8 selectivity even at a high filler loading of 45 wt.%, largely surpassing upper bound limits. This excellent separation performance can be attributed to the successful combination of the molecular sieving properties of KAUST-7 with an enhancement of the interfacial microenvironment in the hybrid membrane by carbene functionalization. Markedly, the optimal MMM exhibits superior anti-plasticization performance for mixed-gas C_3H_6/C_3H_8 separation at a high pressure of up to 8 bar, whereas both pure 6FDA-DAM membrane and the benchmark ZIF-67-based MMM fail to maintain their performance under identical conditions. In addition, the good mechanical strength, decent separation performance at high temperatures of up to 100 °C, and the remarkable long-term stability render KAUST-7-IDip-based MMMs potential candidates for industrial C_3H_6/C_3H_8 applications. It is worth mentioning that membrane configurations also play pivotal roles in the commercialization of promising membrane materials. Hollow fiber modules dominate the current gas separation market owing to their higher packing density and relatively lower production cost compared to spiral wound modules. Therefore, our future efforts will be devoted to the fabrication of asymmetric KAUST-7-IDip-based hollow fiber MMMs with ultrathin selective layers and superior interfacial compatibility. Finally, the simplicity and effectiveness of the carbene functionalization offer potential to extend this approach to other MOF-based MMMs for diversified separation applications, paving the way to rational design of more high-performance MMMs for challenging separations.

Supporting Information

Supporting Information is available from the Wiley Online Library or from the author.

Conflict of Interest

The authors declare no conflict of interest.

Data Availability Statement

The data that support the findings of this study are available from the corresponding author upon reasonable request.

[1] R. W. Baker, B. T. Low, *Macromolecules* **2014**, *47*, 6999.
[2] Y. Wang, S. B. Peh, D. Zhao, *Small* **2019**, *15*, 1900058.
[3] D. S. Sholl, R. P. Lively, *Nature* **2016**, *532*, 435.
[4] a) L. M. Robeson, *J. Membr. Sci.* **1991**, *62*, 165; b) L. M. Robeson, *J. Membr. Sci.* **2008**, *320*, 390.
[5] R. L. Burns, W. J. Koros, *J. Membr. Sci.* **2003**, *211*, 299.
[6] a) Y. Liu, Z. Chen, G. Liu, Y. Belmabkhout, K. Adil, M. Eddaoudi, W. Koros, *Adv. Mater.* **2019**, *31*, 1807513; b) A. Knebel, A. Bavykina, S.

**ADVANCED
SCIENCE NEWS**

www.advancedsciencenews.com

**ADVANCED
MATERIALS**

www.advmat.de

J. Datta, L. Sundermann, L. Garzon-Tovar, Y. Lebedev, S. Durini, R. Ahmad, S. M. Kozlov, G. Shterk, M. Karunakaran, I. D. Carja, D. Simic, I. Weilert, M. Klüppel, U. Giese, L. Cavallo, M. Rueping, M. Eddaoudi, J. Caro, J. Gascon, *Nat. Mater.* **2020**, *19*, 1346; c) O. Kwon, M. Kim, E. Choi, J. H. Bae, S. Yoo, J. C. Won, Y. H. Kim, J. H. Shin, J. S. Lee, D. W. Kim, *Sci. Adv.* **2022**, *8*, eabl6841.

[7] Q. Zhang, H. Li, S. Chen, J. Duan, W. Jin, *J. Membr. Sci.* **2020**, *611*, 118288.

[8] Y. Su, S. Cong, M. Shan, Y. Zhang, *AlChE J.* **2022**, *68*, e17410.

[9] a) C. Zhang, Y. Dai, J. R. Johnson, O. Karvan, W. J. Koros, *J. Membr. Sci.* **2012**, *389*, 34; b) H. An, S. Park, H. T. Kwon, H.-K. Jeong, J. S. Lee, *J. Membr. Sci.* **2017**, *526*, 367; c) T. H. Lee, J. G. Jung, Y. J. Kim, J. S. Roh, H. W. Yoon, B. S. Ghanem, H. W. Kim, Y. H. Cho, I. Pinnau, H. B. Park, *Angew. Chem., Int. Ed.* **2021**, *60*, 13081.

[10] a) J. Dechnik, J. Gascon, C. J. Doonan, C. Janiak, C. J. Sumby, *Angew. Chem., Int. Ed.* **2017**, *56*, 9292; b) Q. Song, S. K. Nataraj, M. V. Roussenova, J. C. Tan, D. J. Hughes, W. Li, P. Bourgoin, M. A. Alam, A. K. Cheetham, S. A. Al-Muhtaseb, E. Sivaniah, *Energy Environ. Sci.* **2012**, *5*, 8359; c) J. E. Bachman, Z. P. Smith, T. Li, T. Xu, J. R. Long, *Nat. Mater.* **2016**, *15*, 845; d) X. Wu, W. Liu, H. Wu, X. Zong, L. Yang, Y. Wu, Y. Ren, C. Shi, S. Wang, Z. Jiang, *J. Membr. Sci.* **2018**, *548*, 309.

[11] A. Cadiau, K. Adil, P. M. Bhatt, Y. Belmabkhout, M. Eddaoudi, *Science* **2016**, *353*, 137.

[12] a) D. Antypov, A. Shkurenko, P. M. Bhatt, Y. Belmabkhout, K. Adil, A. Cadiau, M. Suyetin, M. Eddaoudi, M. J. Rosseinsky, M. S. Dyer, *Nat. Commun.* **2020**, *11*, 6099; b) P. M. Bhatt, Y. Belmabkhout, A. Cadiau, K. Adil, O. Shekhah, A. Shkurenko, L. J. Barbour, M. Eddaoudi, *J. Am. Chem. Soc.* **2016**, *138*, 9301.

[13] a) Q. Xin, J. Ouyang, T. Liu, Z. Li, Z. Li, Y. Liu, S. Wang, H. Wu, Z. Jiang, X. Cao, *ACS Appl. Mater. Interfaces* **2015**, *7*, 1065; b) K. Xie, Q. Fu, J. Kim, H. Lu, Y. He, Q. Zhao, J. Scofield, P. A. Webley, G. G. Qiao, *J. Membr. Sci.* **2017**, *535*, 350; c) Z. Wang, D. Wang, S. Zhang, L. Hu, J. Jin, *Adv. Mater.* **2016**, *28*, 3399.

[14] D. Poloneeva, S. J. Datta, L. Garzon-Tovar, S. Durini, M. Rueping, M. Eddaoudi, A. Bavykina, J. Gascon, *Acc Mater Res* **2021**, *2*, 1133.

[15] Y. Cheng, Y. Ying, S. Japip, S.-D. Jiang, T.-S. Chung, S. Zhang, D. Zhao, *Adv. Mater.* **2018**, *30*, 1802401.

[16] H. An, K. Y. Cho, Q. Lyu, D.-S. Chiou, K. J. Nam, D.-Y. Kang, L.-C. Lin, J. S. Lee, *Adv. Funct. Mater.* **2021**, *31*, 2105577.

[17] a) Y. Cheng, Y. Ying, L. Zhai, G. Liu, J. Dong, Y. Wang, M. P. Christopher, S. Long, Y. Wang, D. Zhao, *J. Membr. Sci.* **2019**, *573*, 97; b) S. J. Datta, A. Mayoral, N. M. S. Bettahalli, P. M. Bhatt, M. Karunakaran, I. D. Carja, D. Fan, P. G. M. Mileo, R. Semino, G. Maurin, O. Terasaki, M. Eddaoudi, *Science* **2022**, *376*, 1080.

[18] Z. Wang, W. Wang, T. Zeng, D. Ma, P. Zhang, S. Zhao, L. Yang, X. Zou, G. Zhu, *Adv. Mater.* **2022**, *34*, 2104606.

[19] G. Liu, V. Chernikova, Y. Liu, K. Zhang, Y. Belmabkhout, O. Shekhah, C. Zhang, S. Yi, M. Eddaoudi, W. J. Koros, *Nat. Mater.* **2018**, *17*, 283.

[20] Y. Cheng, L. Zhai, Y. Ying, Y. Wang, G. Liu, J. Dong, D. Z. L. Ng, S. A. Khan, D. Zhao, *J. Mater. Chem. A* **2019**, *7*, 4549.

[21] N. C. Su, D. T. Sun, C. M. Beavers, D. K. Britt, W. L. Queen, J. J. Urban, *Energy Environ. Sci.* **2016**, *9*, 922.

[22] J. G. Wijmans, R. W. Baker, *J. Membr. Sci.* **1995**, *107*, 1.

[23] C. Ma, J. J. Urban, *Adv. Funct. Mater.* **2019**, *29*, 1903243.

[24] S. Zhou, O. Shekhah, J. Jia, J. Czaban-Jóźwiak, P. M. Bhatt, A. Ramírez, J. Gascon, M. Eddaoudi, *Nat. Energy* **2021**, *6*, 882.